Neurobiology of Disease 141 (2020) 104938

Contents lists available at ScienceDirect

Neurobiology of Disease

journal homepage: www.elsevier.com/locate/ynbdi

Characterization of a new molecule capable of inhibiting several steps of the amyloid cascade in Alzheimer's disease

Christian Peters[a,1,2], Denisse Bascuñán[a,2], Carlos F. Burgos[a], Catalina Bobadilla[a], Juliana González-Sanmiguel[a], Subramanian Boopathi[b], Nicolás Riffo[a], Eduardo J. Fernández-Pérez[a], María Elena Tarnok[d], Luis Felipe Aguilar[d], Wendy Gonzalez[b,c], Luis G. Aguayo[a,*]

[a] Laboratory of Neurophysiology, Department of Physiology, Universidad de Concepción, Concepción, Chile
[b] The Center for Bioinformatics and Molecular Simulations (CBSM), Universidad de Talca, Talca, Chile
[c] Millennium Nucleus of Ion Channels-Associated Diseases (MiNICAD), Universidad de Talca, Talca, Chile
[d] Laboratory of Photophysics and Molecular Spectroscopy, Chemistry, Pontificia Universidad Católica de Valparaíso, Valparaíso, Chile

ARTICLE INFO

Keywords:
Alzheimer
Small molecule
Novel
Multi-step
Drug
Therapy

ABSTRACT

Introduction: Alzheimer's disease (AD) is the most prevalent neurodegenerative disorder in elderly people. Existent therapies are directed at alleviating some symptoms, but are not effective in altering the course of the disease.

Methods: Based on our previous study that showed that an Aβ-interacting small peptide protected against the toxic effects of amyloid-beta peptide (Aβ), we carried out an array of *in silico, in vitro,* and *in vivo* assays to identify a molecule having neuroprotective properties.

Results: In silico studies showed that the molecule, referred to as M30 (2-Octahydroisoquinolin-2(1H)-ylethanamine), was able to interact with the Aβ peptide. Additionally, *in vitro* assays showed that M30 blocked Aβ aggregation, association to the plasma membrane, synaptotoxicity, intracellular calcium, and cellular toxicity, while *in vivo* experiments demonstrated that M30 induced a neuroprotective effect by decreasing the toxicity of Aβ in the dentate gyrus of the hippocampus and improving the alteration in spatial memory in behavior assays.

Discussion: Therefore, we propose that this new small molecule could be a useful candidate for the additional development of a treatment against AD since it appears to block multiple steps in the amyloid cascade. Overall, since there are no drugs that effectively block the progression of AD, this approach represents an innovative strategy.

Significance: Currently, there is no effective treatment for AD and the expectations to develop an effective therapy are low. Using *in silico, in vitro,* and *in vivo* experiments, we identified a new compound that is able to inhibit Aβ-induced neurotoxicity, specifically aggregation, association to neurons, synaptic toxicity, calcium dyshomeostasis and memory impairment induced by Aβ. Because Aβ toxicity is central to AD progression, the inhibition mediated by this new molecule might be useful as a therapeutic tool.

Abbreviations: Alzheimer's disease, (AD); Amyloid-beta peptide, (Aβ); Amyloid-beta peptide 1–42, ($Aβ_{1-42}$); 2-Octahydroisoquinolin-2(1H)-ylethanamine, (M30); C-terminal region of Aβ, (Aβ-CT); Loop region of Aβ, (Aβ-LP); ADME, (absorption, distribution, metabolism, elimination); Aβ-6-carboxyfluorescein, (Aβ-FAM); Synaptic vesicle protein 2, (SV2); Mitochondrial oxidative phosphorylation uncoupler, (FCCP); 3-(4,5-dimethylthiazol-2-yl)-2,5-diphenyltetrazolium bromide, (MTT); Nuclear Magnetic Resonance, (NMR); High-throughput screening, (HTS); Days *in vitro*, (DIV); Minimal essential medium, (MEM); Hexafluoroisopropanol, (HFIP); Central nervous system, (CNS); Root-mean-square deviation, (RMSD); Anterior-posterior, (AP); Medial-lateral, (ML); DV, (Dorsal-ventral); Calcein-AM and Ethidium homodimer-1, (EthD-1); PBS, (Phosphate-Buffered Saline); EDTA, (Ethylenediaminetetraacetic acid); DTT, (Dithiothreitol); DMSO, (Dimethyl Sulfoxide)

* Corresponding author.
E-mail address: laguayo@udec.cl (L.G. Aguayo).
[1] Current address. Molecules-Signaling-Development, Max Planck Institute of Neurobiology, Martinsried, Germany.
[2] These authors contributed equally to this work.

https://doi.org/10.1016/j.nbd.2020.104938
Received 3 April 2020
Available online 18 May 2020

1. Introduction

In the quest for the development of new pharmacotherapeutics to treat AD, these compounds ideally should be able to modify its course by interfering with one of the most toxic agents of the disease, Aβ. Current treatments are aimed at alleviating some symptoms of the disease but are not effective in modifying the disease, and patients continue with progressive cognitive deficits (Salomone et al., 2012). Thus, the cellular target where Aβ exerts its toxic effect is not known and prevents the development of an effective treatment. Furthermore, it is believed that early symptoms of AD, such as confusion and memory loss, are likely associated to synaptic alterations caused by Aβ oligomers (Shankar et al., 2007).

We previously found that a small peptide derived from an amino acid sequence of Aβ (GLMVG) interacted with the C terminal region of Aβ and blocked its aggregation, association, and perforation of the neuronal membrane, and also prevented changes in intracellular calcium levels and the synaptotoxicity induced by Aβ (Peters et al., 2013). Based on these findings, we are now searching for a low molecular weight compound that can interact and inhibit the toxicity of Aβ because it is the principal toxic agent in AD (Jin et al., 2011; Sandberg et al., 2010). Using a virtual screening based on the C-terminal region of Aβ as the "receptor", we identified a set of small molecules with the capacity to associate to this region. The most active compound as determined by secondary assays, referred to as M30, was used to perform a detailed characterization in the present study. To be effective, any suitable compound must have a number of pharmacokinetic properties for its use as a drug in the central nervous system. For example, it should consider Lipinski's rule of five (Lipinski et al., 2001) or Jorgensen's rule of three (Jorgensen and Duffy, 2002), have an ability to cross the blood-brain barrier (Kelder et al., 1999), a potential activity in the central nervous system (Ajay et al., 1999), and not be extensively metabolized. Additionally, the filters must be used to select compounds with an acceptable range to evaluate drug-likeness. *In silico* methodologies have already been used to identify molecules that inhibit processes of different diseases (Grover et al., 2014; Veeramachaneni et al., 2015). Here we describe the first compound we found that interferes with several toxic steps in the amyloid cascade (Fig. 1), the molecule M30 (2-Octahydroisoquinolin-2(1H)-ylethanamine).

2. Results

The experimental approach included the sequential use of *in silico*, *in vitro* and *in vivo* studies. The goal was to identify and characterize a novel small molecule capable of antagonizing the toxicity of Aβ.

2.1. In silico

To circumvent the disadvantages of using peptides in pharmacotherapy, we wanted to identify low molecular weight compounds that can interact with the same region where GLMVG blocks Aβ toxicity and could be used in pharmacotherapy (Peters et al., 2013). Initially, the docking simulation with the Aβ monomer grid centered on the C-terminal region (Aβ-CT) and the library of filtered molecules was performed in the SP precision of Glide. Once the docking with the Aβ monomer was completed, 2,425,934 complexes equivalent to 89.7% of the filtered molecules were obtained. The remaining 279,137 molecules (10.3%) were unable to generate stable poses with the interaction grid. Subsequently, all the complexes were ordered according to the docking score value, and ΔG_{bind} (MM-GBSA) was calculated for the best 1000 molecules. The combination of the *in silico* results with preliminary primary assays allowed us to select a single molecule (M30, 2-Octahydroisoquinolin-2(1H)-ylethanamine (Fig. 2A)) that showed the best protective activity in all performed assays. The data showed that this molecule interacted stably with the C-terminal portion of the Aβ monomer presenting a docking score of −6.096 (Fig. 2B). A more

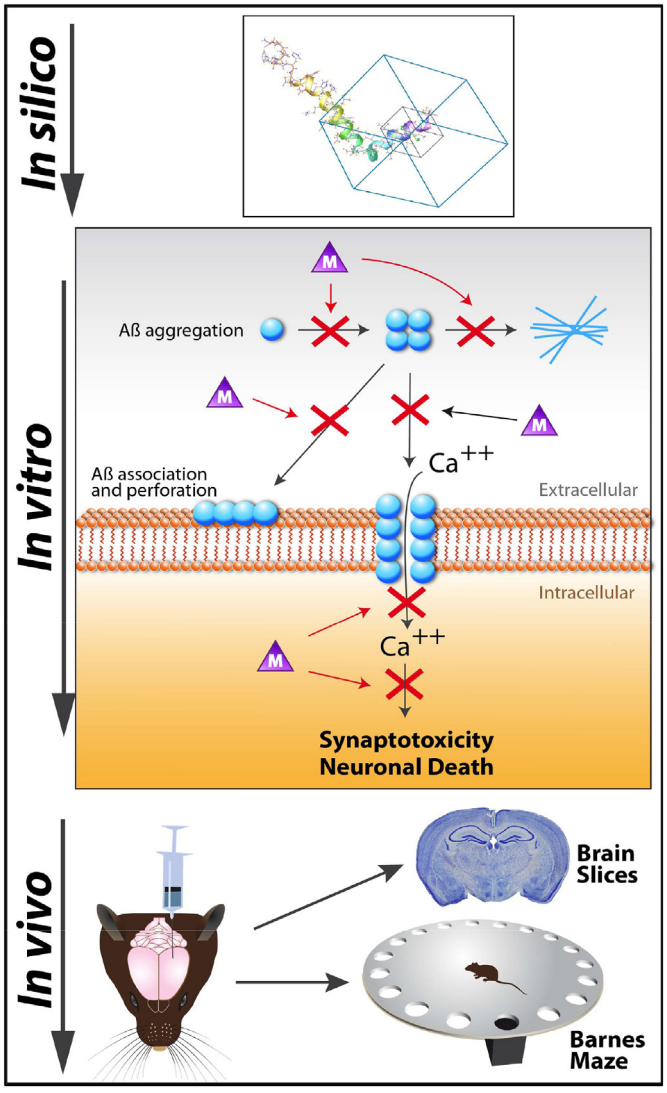

Fig. 1. Scheme of the experimental approach used to identify novel anti AD drugs. *In silico:* The blue box represents the grid used to identify small molecules interacting with the C-terminal region of $A\beta_{1-42}$. These molecules were selected from the ZINC database using a set of filters to identify those having better CNS pharmacological properties. *In vitro:* We evaluated selected molecules on Aβ aggregation, association, perforation of the membrane, and synaptotoxicity in hippocampal neurons. Aβ is represented as pale blue circles and the molecules as purple triangles (M). The M30 compound was the most active in inhibiting the toxic effects of Aβ in most primary assays and exhibited good ADME parameters. *In vivo:* Stereotaxic injection of Aβ into the mouse dentate gyrus was used to evaluate neuronal toxicity *in vivo* after 2 weeks post-surgery. Moreover, a memory-learning test, the Barnes Maze, was used to assess the protective effects of the molecules in the mice. (For interpretation of the references to colour in this figure legend, the reader is referred to the web version of this article.)

detailed analysis of the interface revealed that between M30 and the Aβ monomer 2 hydrogen bonds were formed between the NH groups of the molecule and the carboxyl and hydroxyl groups of the main chains of amino acids valine 39 and alanine 42, respectively. A salt bridge between M30 and alanine 42 was also detected in the interaction (Fig. 2C). For the selected molecule, a second protein-ligand docking was performed using a grid that evaluated the remaining Aβ monomer, especially the central loop that was associated with the folding changes in the aggregation process (Aβ-LP). M30 was able to interact favorably with the Aβ monomer in the region near the hinge generating a docking score of −5256 and involving amino acids valine 18, alanine 21,

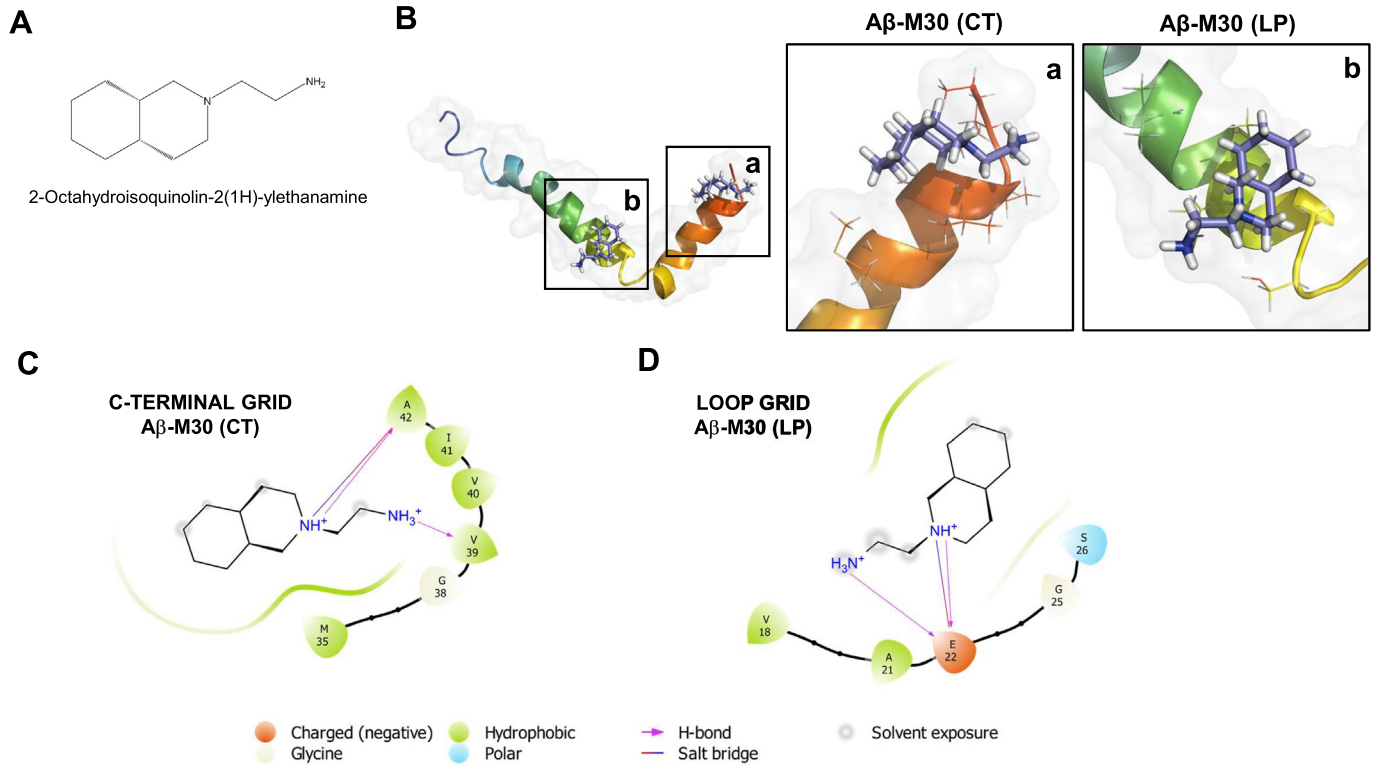

Fig. 2. Docking between M30 and Aβ monomer. (A) Chemical structure of M30. (B) M30-Aβ complexes generated by molecular docking for the C-terminal (a) and the loop regions (b). The zooms shown on the right side correspond to the side chains of the amino acids involved and are represented as lines. (C, D) Schematic representation of M30 interactions with Aβ. Predictions were generated with the structure obtained by PDB 1IYT. Ligand-interaction diagram of complexes between M30 and Aβ, where (C) corresponds to the C-terminal grid, while (D) to the central grid. The legend of the schemes is common for both interaction grids.

glutamic acid 22, glycine 25 and serine 26 in the binding site (Fig. 2D). In the interface of this second binding site, we detected the formation of two hydrogen bonds and a salt bridge with glutamic acid 22 of Aβ (Fig. 2D). Both complexes had favorable ΔG_{bind} values (−26.428 kcal/mol C-terminal grid; −31.687 kcal/mol central grid) which, together with the aforementioned, confirmed an *in silico* interaction between M30 and Aβ. These structural and energetic properties add to the previously calculated ADME parameters, known as the critical pharmacokinetic hurdles (absorption, distribution, metabolism, elimination) that a drug must address before being approved by the FDA for clinical use (Supplementary Table 1), that indicated that M30 is a potential candidate to inhibit the toxic effects of the Aβ peptide.

2.2. Molecular dynamics analysis between Aβ and M30

To improve the predictions for binding of M30 to the Aβ peptide, we performed molecular dynamics simulations on Aβ, and the complexes Aβ-M30/CT and Aβ-M30/LP, in explicit water molecules over 1 μs. The Aβ peptide was divided into five regions for the analysis: 1) N-terminal (Asp1-Lys16), 2) central hydrophobic core (Leu17-Ala21), 3) loop region (Glu22-Lys28), 4) second hydrophobic core (Phe29-Met35), and 5) C-terminal region (Val36-Ala42). Although M30 was initially located in the docking simulation in the LP and the CT poses, this was able to closely interact with the entire Aβ peptide (Fig. 3A). Analysis of the secondary structure along the simulations showed that Aβ had ~10.22% of β-sheet, ~13.50% of helix, ~20.52% of turns and ~ 55.75% of coils (Supplementary Table 2, Fig. 3B). The averaged helical content was reduced to ~8.72% and ~ 10.86% in the case of Aβ–M30 (LP) and Aβ-M30 (CT), respectively. Additionally, a reduction in the content of β-sheet to 7.03% was detected in the Aβ-M30 (LP) complex. The decrease in the β-sheet content in the case of Aβ–M30 (LP) can be associated to prevention of Aβ self-assembly and aggregation, where the propensity of β-sheet formation at region Leu17-Met35 changed from 11.2% to 6.5% in the presence of M30 (Fig. 3B). These results indicate that M30 was able to modify the secondary structure of Aβ, with a tendency to reduce the formation of β-sheet structures. This was also accompanied by a decrease in intramolecular interactions (Fig. S2). Taken together, the *in silico* results indicate that M30 is able to interact and modify the structural properties of Aβ reducing its toxicity.

2.3. Aβ structure and aggregation

It is well known that Aβ aggregation forms β-sheet structures (O'Nuallain et al., 2010; Riek and Eisenberg, 2016). Circular dichroism experiments confirmed that after aggregation, Aβ was chiefly composed of β-sheet structures (Fig. 4A). As we showed with *in silico* analysis, M30 was able to affect Aβ, and this likely molecular interaction resulted in changes in Aβ aggregation and alteration in the secondary structure of Aβ oligomers or fibers. Indeed, M30 was able to reduce the β-sheet content of 1 μM Aβ after co-incubation with two different concentrations (5 and 10 μM) (Fig. 4A). To confirm that the changes observed in Aβ spectra were not due to peptide precipitation, we monitored the protein present in the cuvette by absorbance, before and after adding M30, and found no significant changes between the samples of Aβ with and without M30. This suggests that the observed change in circular dichroism was related to a change in the secondary structure of the peptide. From this data, we concluded that the main change in Aβ structure was from antiparallel β-sheets to other structures, and no alpha helix structures were found in all tested conditions (Table supplementary 3).

The change in the secondary structure of Aβ could be related to alterations in the aggregation by M30. Therefore, we next examined if M30 was able to alter the aggregation of Aβ oligomers measured as the change in absorbance ($\Delta Abs/Abs_{time0}$). The data obtained with this approach showed that Aβ aggregation (32 μM; red) was inhibited in the presence of M30 (160 μM; blue) (Fig. 4B). To maintain the 1:5 Aβ:M30

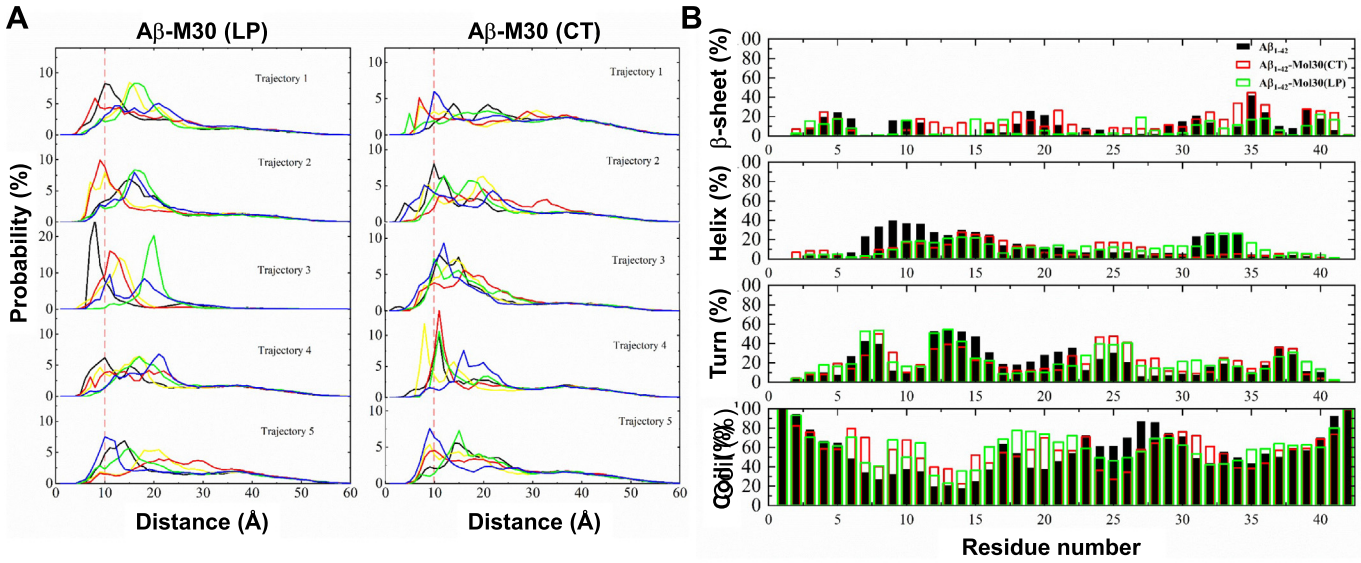

Fig. 3. Molecular dynamics show the distance distribution between M30 and various regions of Aβ-M30(LP) and Aβ-M30(CT). (A) The Aβ sequence was divided into five regions colored according to the following order: black line, N-terminal (NT, aa 1–16); yellow line, central hydrophobic core (CHC, 17–21); red line, loop region (LP, 22–28); green line, second hydrophobic core (SHC, 29–35); and blue line, C-terminal (CT, 36–42). The vertical red dotted line at 10 Å represents contacts between Aβ and M30. (B) Averaged per-residue secondary structure contents for Aβ, Aβ-M30(LP) and Aβ-M30(CT) calculated by DSSP. (For interpretation of the references to colour in this figure legend, the reader is referred to the web version of this article.)

ratio used in the CD study, the corresponding concentration of M30 was 160 μM.

2.4. Inhibition of Aβ association to neuronal membranes in the presence of M30

Next, we evaluated if M30 was able to decrease Aβ association to PC12 cells and hippocampal neurons (Fig. 5, and S3). To assess this, we first performed a dot blot assay to determine the level of association of Aβ with PC12 cells for a 60 min treatment (5 μM), in the absence and presence of 25 μM M30 (Fig. 5A). Quantification of the data obtained from 6 different experiments showed a significant reduction in the association of Aβ (Fig. 5B, $^{**}p < .01$). Moreover, western blot analysis also showed a similar reduction in Aβ association to neurons after 1 h incubation, while another molecule (M29) did not show this effect (Fig. S3). This reduction of Aβ association was confirmed with studies in hippocampal neurons. Using confocal microscopy and fluorescent Aβ, we found that the association of Aβ-6-carboxyfluorescein (1 μM Aβ-FAM, green) was reduced in the presence of M30 (Fig. 5C). For these analyses, the neurons were identified using an antibody that recognized MAP2, a neuronal protein (red). The data show that the intensity and the number of Aβ punctas associated with the neurons was reduced by 5 μM M30 (Fig. 5 D,E, $p < .05$.; *** $P < .001$, $n = 4$). Specifically, there was a significant reduction in these two parameters in primary processes (length 20 μm) when the neurons were treated with the compound.

2.5. M30 inhibited the increase in intracellular calcium induced by Aβ oligomers

Our working model for neurotoxicity involves an association of Aβ to the membrane that causes membrane disruption and is followed by an increase in intracellular calcium and synaptotoxicity (Parodi et al., 2010; Peters et al., 2016; Peters et al., 2013). Therefore, we examined if M30 was able to interfere with the increase in intracellular calcium induced by application of Aβ (5 μM) to PC12 cells (Fig. 6). Compared with ionomycin (10 μM), a well-known membrane permeabilizing compound, we found that Aβ, although to a lower level, also increased the level of intracellular calcium, as monitored by the change in Fluo-8 fluorescence (Fig. 6A). Application of M30 was able to attenuate the effect of Aβ during the time course of the experiment (Fig. 6B), and the bar graph shows the changes at 25 min of application in the absence and presence of M30 (Fig. 6C, $p < .001$, $n = 3$).

2.6. M30 inhibited the synaptoxicity induced by Aβ oligomers in hippocampal neurons

It was previously shown that Aβ oligomers are synaptotoxic, as reflected by a reduction in the levels of the synaptic vesicle protein 2 (SV2) and the synaptic activity of the neurons (Peters et al., 2015; Peters et al., 2013). Here, we used western blot and immunocytochemistry analyses to evaluate SV2 levels in hippocampal neurons. The results obtained by western blot show that treatment with Aβ (1 μM) reduced the level of SV2 to about 50% of control and that M30 (5 μM) was able to block this Aβ-induced synaptotoxicity (Fig. 7A and B, $p < .005$, $n = 4$). Furthermore, confocal microscopy confirmed that M30 decreased the reduction in the SV2 signal in presence of Aβ (Fig. 7C), as measured by intensity (Fig. 7D) and number of punctas (Fig. 7E) in the primary processes of these neurons. The synaptic alterations produced by long-term treatment of hippocampal neurons with Aβ is accompanied by a reduced number of spontaneous intracellular calcium transients (Peters et al., 2015). Therefore, we measured the frequency of calcium transients after chronic treatments with Aβ in hippocampal neurons (Fig. 7F) finding that Aβ decreased the frequency and that M30 blocked this synaptotoxic effect (Fig. 7G). The data also showed that M30 did not cause any effect on its own in spontaneous calcium transients, reflecting unaltered synaptic functions. Moreover, to further evaluate if M30 antagonized Aβ effects, we treated hippocampal neurons with Aβ (1 μM) in the presence or absence of 1 μM M30 and recorded the total synaptic activity using voltage clamp (Fig. 7H). Interestingly, and in agreement with the effects on frequency of calcium transients, M30 blocked the decrease in synaptic transmission after exposure of neurons to Aβ (Fig. 7I). Once again, the compound alone did not have any effect altering neurotransmission.

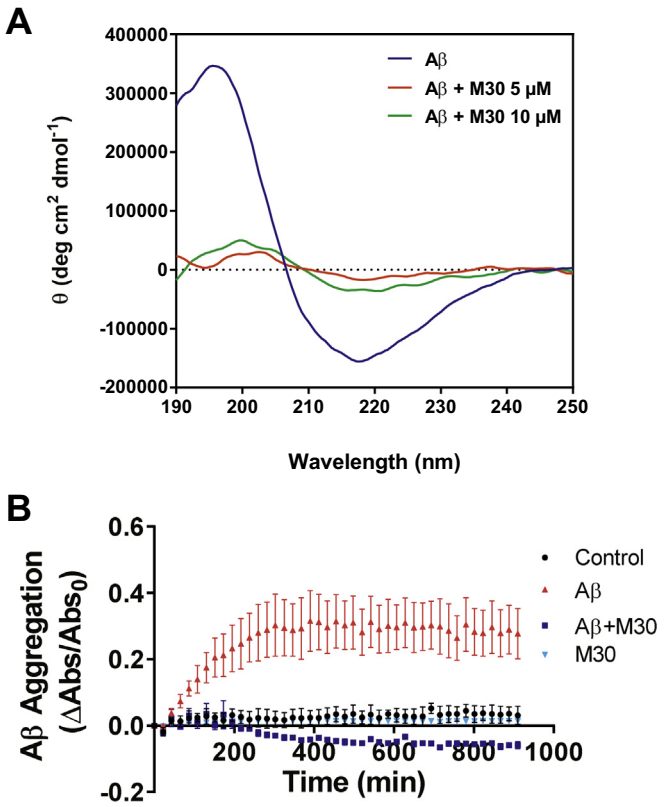

Fig. 4. The β-sheet structure of Aβ was altered by M30. (A) Circular dichroism spectra of 1 μM Aβ aggregated alone and in the presence of 5 μM and 10 μM M30 for 24 h at 4 °C. The control condition demonstrated the β-sheet structure of Aβ (blue line). Co-incubation with 5 μM (red line) and 10 μM M30 (green line) showed a significant change in β-sheet secondary structure of the peptide. (B) Absorbance measurements showing the aggregation curve of Aβ oligomers (red, 32 μM) after incubation at 37 °C for 16 h, with or without M30 (160 μM). The assay was started with pre-aggregated oligomers and the data is represented as the normalization of $\Delta Abs/Abs_0$. The control is the vehicle alone. The data of Aβ with and without M30 displayed $p < .001$ for most points. (For interpretation of the references to colour in this figure legend, the reader is referred to the web version of this article.)

2.7. Effect of M30 on mitochondrial function and cellular viability toxicity induced by Aβ

To evaluate if M30 inhibited the Aβ induced cytotoxicity after chronic treatment, we assayed mitochondrial function using an MTT assay together with cell viability using the live/dead assay. After a 24 h treatment with Aβ alone (1 μM), the MTT (3-(4,5-dimethylthiazol-2-yl)-2,5-diphenyltetrazolium bromide) assay showed a significant reduction in mitochondrial function, an effect that was significantly attenuated by co-treatment with M30 (5 μM, $^{***}p < .001$, $n = 6$). M30 by itself did not alter mitochondrial function, and FCCP, a mitochondrial oxidative phosphorylation uncoupler, decreased mitochondrial status to less than 20% of control (Fig. 8A). The live/dead assay showed that hippocampal neuron viability was reduced to ≈60% with long exposures to Aβ (96 h). The cytotoxic effect of the peptide was blocked by increasing concentrations (1–50 μM) of M30 (Fig. 8B). Interestingly, M30 was not able to block the toxicity induced by FCCP, showing a degree of specificity for protection only against Aβ under the experimental conditions (Fig. 8C). The data also showed that high concentrations of M30 (25–50 μM) did not alter cellular viability (Fig. 8D). Finally, we determined an IC_{50} for M30 of 680 ± 9 nM to block the toxicity of Aβ (Fig. 8E).

2.8. Neuronal death and memory impairment was antagonized by M30 in vivo

After determining that M30 interacted *in silico* with Aβ and protected the synapsis in *in vitro* experiments, it was necessary to examine if the compound was also effective in *in vivo* studies. It was previously reported that direct infusion of oligomeric Aβ into the brain of wild-type mice provides a rapid approach that replicates several neuronal death aspects related to amyloidopathy (Jean, 2015) (Baleriola et al., 2014). In agreement, 2 weeks after the stereotaxic injection of Aβ into the dentate gyrus (DG) of the mouse hippocampus (Fig. 9 A-C), a decrease in DAPI-positive staining was found (Fig. 9D,*E*). After injection of Aβ-FAM into the left hemisphere, and Aβ-FAM plus M30 into the right hemisphere, the results showed a reduction in the Aβ-FAM signal into the right hemisphere (with M30) after 2 weeks (Fig. 9F and S4). Analysis of DAPI-positive cells in the hemisphere injected with Aβ + M30 showed a decrease in cell death induced by Aβ (Fig. 9G-I).

Finally, we performed the Barnes Maze assay, a spatial memory test (Webster et al., 2014), to examine if mice injected with Aβ plus M30 have less impairment than those injected with Aβ alone (Fig. 10A). The data showed that the mice that received the administration of Aβ plus M30 in the DG showed better spatial learning after 1 week post-injection (Fig. 10B). The data shows that the percentage of animals reaching the exit within the 3 min time frame of the assay was significantly higher in those injected with Aβ + M30 than in Aβ alone, showing similar values with the control group (Fig. 10C). Additionally, the latency, or time that the mice took to reach the exit, was higher in the mice injected with Aβ than control and Aβ + M30 animals (Fig. 10D).

3. Discussion

3.1. Rationale and justification for the use of small molecular weight molecules

The global increase in the aging population is resulting in more cases of Alzheimer's disease (AD), increasing the social and economic burdens associated to this disorder. For the last 30–40 years, the high prevalence and lack of effective therapies to treat AD have led scientists to search for several potential targets that can block the neurotoxic effects of Aβ. Given the high complexity of the pathophysiology of AD and our limited knowledge about the biological basis of the disease, it has been difficult to develop a small-molecule therapy that can reliably prevent and/or treat this disease. The principal chemical entities described to date correspond to inhibitors of Aβ oligomerization, secretase inhibitors that process APP, vaccines that neutralize Aβ, and trace metal chelators (Carreiras et al., 2013; De Strooper and Chavez Gutierrez, 2015; Trippier et al., 2013). They all have limited symptomatic effects, but none show the ability to modify the course of AD (Salomone et al., 2012).

In a previous study, we identified a small peptide derived from the C-terminal region of Aβ that interfered with a myriad of toxic effects induced by Aβ (Peters et al., 2013). Nevertheless, although peptide-based pharmacotherapies have been used for some time (Banting et al., 1922), there are limitations in their use. For example, peptidases and excretory mechanisms decrease the half-life of many peptidergic hormones (Lau and Dunn, 2018). Likewise, the availability of peptidergic compounds is reduced by enzymes in the gastrointestinal tract that cleave peptidic bonds, and the high polarity and molecular weight limit intestinal permeability (Lau and Dunn, 2018). Injectable formulations, on the other hand, reduce patient compliance in chronic therapy. Small molecules are generally more suitable for oral delivery and easier to manufacture than peptides, and additionally new high-throughput screening (HTS) technologies are shifting the direction towards small molecules that target peptide-related receptors (Lau and Dunn, 2018). Small molecules can also be useful to interfere with Aβ oligomers because, unlike monomeric Aβ which does not have a defined structure,

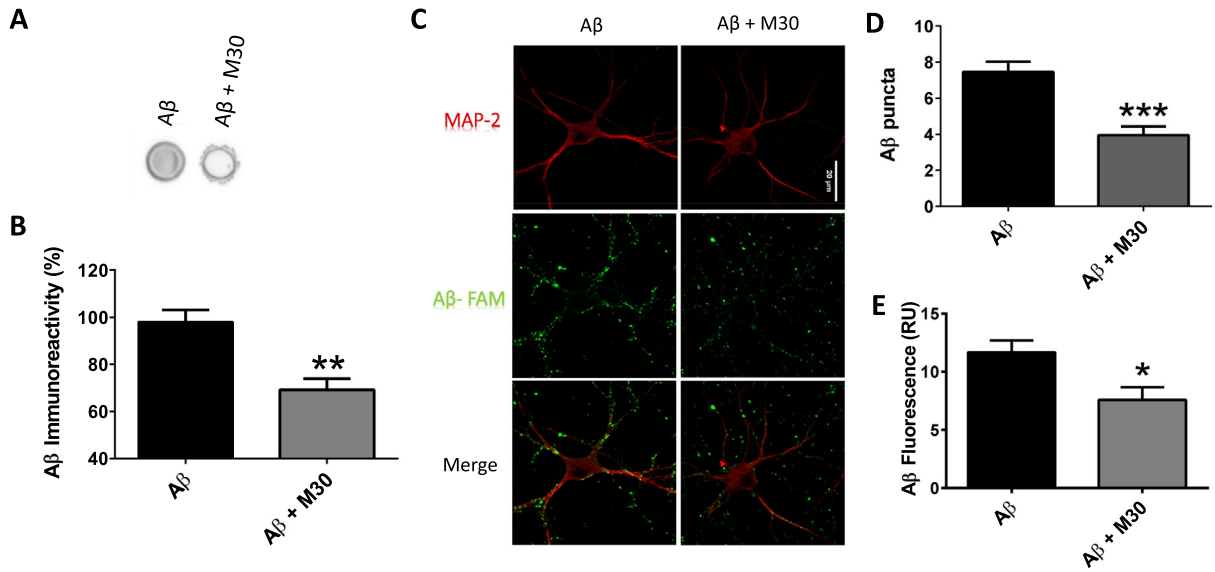

Fig. 5. M30 reduced Aβ association to PC12 cells and neurons. (A) Dot blot obtained from PC12 culture lysates that show Aβ (1 h, 5 μM) association in the absence or presence of M30 (25 μM). (B) Quantification of Aβ association to PC 12 cells from A. $n = 6$ (C) The confocal microscopy images were obtained in hippocampal neurons treated for 60 min with 1 μM Aβ-FAM (green punctae) in absence and presence of M30. To identify the Aβ associated to the neurons, immunofluorescence with MAP2 (red) was used. (D, E) Quantification of Aβ puncta number per 20 μm of the neuronal primary process and fluorescence intensity. Data obtained in Aβ from 43 primary processes (20 neurons) and in Aβ + M30 from 17 primary processes (10 neurons). $^{*}p < .5$; $^{**}p < .01$; $^{***}p < .001$. (For interpretation of the references to colour in this figure legend, the reader is referred to the web version of this article.)

they are highly structured and have hydrophobic pockets that can be easily tagged by small molecules such as M30 (Autiero et al., 2013).

With this goal in mind, we have characterized a compound having multiple effects on the amyloid cascade such as aggregation, association, synaptotoxicity, intracellular calcium dyshomeostasis and behavioral impairments.

3.2. Identification of a small molecule derived from an inhibitory pentapeptide

A previous study showed that a small peptide (GLMVG) interacted with Aβ and inhibited several steps in the amyloid cascade (Peters et al., 2013). The present docking and molecular dynamics results strongly suggest that M30 interacts with the whole peptide molecule resulting in a reduction in β-sheet content in the Aβ peptide. Previous data with solid-state NMR revealed that residues from 17 to 35 contributed to the β-sheet formation important for aggregation (Colvin et al., 2016; Tycko, 2011). Interestingly, the β-sheet content from Aβ and Aβ–M30(CT) were consistent with the experimental β-sheet content calculated by NMR and CD studies (Bitan et al., 2003; Huang et al., 2000; Ono et al., 2009) that showed that the experimental β-sheet content (15–25%) was greater than what we found for Aβ–M30(LP). Beta sheet formation is a product of two types of forces: a) hydrophobic contacts between the central hydrophobic and the second hydrophobic regions and interactions between the C-terminal and the N-terminal regions, and b) formation of more stable salt-bridges between Asp23(Glu22) and Lys28 residues. The hydrophobic contacts and salt-bridge formations play a significant role in the formation of Aβ structures with an increased content in β-sheets, which promotes aggregation. Interestingly, M30 binding to Aβ reduced the population of the Asp23-Lys28 and Glu22-Lys28 salt bridges and altered contacts between the central hydrophobic and the second hydrophobic regions, as well as between the C-terminal and the N-terminal regions. Hence, the break-up of the contacts and the destabilization of the salt bridges are main causes for diminishing the β-sheet content and preventing Aβ aggregation, in agreement with experimental observations. These results indicate that M30 was able to modify the secondary structure of Aβ, with a tendency to reduce the formation of β-sheet structures. Taken together, the *in silico* results suggest that M30 is able to interact and modify the structural properties of Aβ reducing its toxicity. Nevertheless, future binding studies will be necessary to confirm our conclusions that are based on *in silico* results.

3.3. Biological evidence supporting an inhibitory effect of M30 on Aβ toxicity

The results showed that M30 blocked the aggregation of Aβ, which is in accordance with the effect of a small molecule in altering the β-sheet structure of Aβ. This could be the basis for neuroprotective effects of M30 in blocking Aβ toxicity since previous work showed that β-sheet oligomers are the most toxic species of Aβ (Guivernau et al., 2016; Sakono and Zako, 2010). In fact, M30 decreased the association of Aβ with PC12 cells and hippocampal primary neurons, and *in vivo*, reduced the acute increase in intracellular calcium induced by Aβ (Fig. 7) that leads to vesicular depletion after chronic Aβ exposure (Parodi et al., 2010; Sepulveda et al., 2010). The capacity of M30 to block several steps of the amyloid cascade was noteworthy. For example, it prevented the decrease in synaptic protein SV2, calcium transients and synaptic neurotransmission. Thus, the synaptotoxic effect of Aβ application was blocked with M30, demonstrating its multi-level blocking properties.

Stereotaxic injection of Aβ into the brain provides an *in vivo* model of amyloidosis, replicating in only a few weeks the neuronal death commonly found in AD (Baleriola et al., 2014; Jean, 2015). Injection of Aβ allowed us to increase its levels in a spatial and temporal fashion obtaining results for neuronal death and memory impairment by Aβ. On the other hand, transgenic mice models require long-term treatment (several months). M30 decreased cell death and Aβ association at the site of injection suggesting that it could be of value for additional screening of compounds with the ability to interfere with the toxic effects of Aβ. The results of our behavioral experiments confirmed that Aβ injections into the DG decreased spatial memory and learning and that this behavior was reverted by M30.

Finally, we believe that the results of this study are significant since currently there are no active compounds with good efficacy to treat AD. Therefore, the use of small molecules like the one described here that is directed against the main toxic biochemical component of the disease

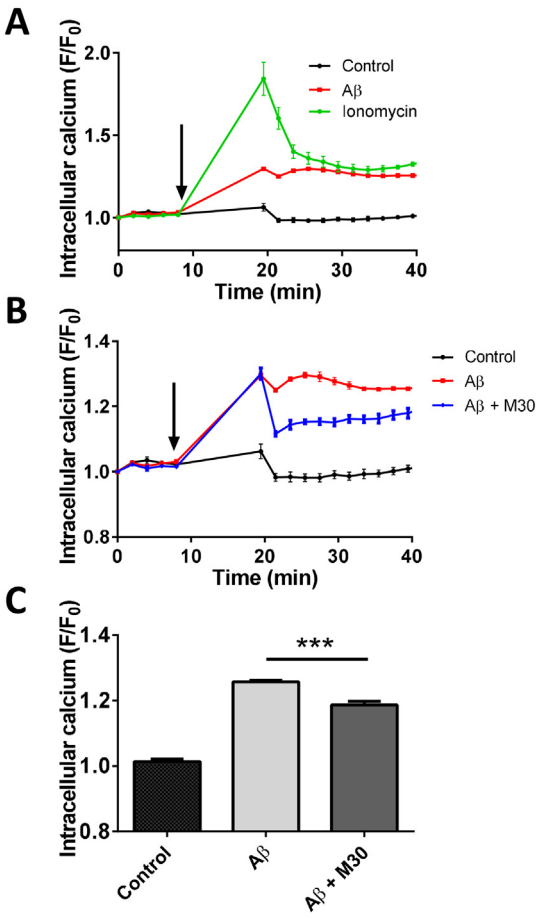

Fig. 6. M30 attenuated the increase in intracellular Ca^{2+} induced by Aβ in PC12 cells. (A) The data show changes in the intensity of fluorescence for fluo-8 indicator under control conditions (vehicle), in presence of Aβ (5 μM) and ionomycin (10 μM, as positive control). (B) The data shows changes in intracellular calcium after treatment with Aβ (5 μM) alone or with M30 (25 μM). (C) The data represent values of fluorescence derived from data in panel B, measured at 25 min after the application of Aβ alone or with M30. ***$p < .001$, $n = 3$.

opens new possibilities for the future development of treatments in the fight against Alzheimer's disease.

4. Materials and methods

4.1. Cell cultures

All animals were handled in strict accordance with NIH guidelines and approved by the Ethics Committee of the Universidad de Concepción (Concepción, Chile). Primary cultures of rat hippocampal neurons were obtained from 18-day pregnant Sprague-Dawley rats and maintained for 10–14 days *in vitro* (DIV) as previously described (Aguayo and Pancetti, 1994). Briefly, the neuronal feeding medium consisted of 90% minimal essential medium (MEM; BRL Technologies, Rockville, MD), 5% heat-inactivated equine serum, 5% fetal bovine serum, and a mixture of nutrient supplements. Cells were maintained with 5% CO_2 at 37 °C.

PC12 cell lines (ATCC, Manassas, VA, USA) were cultured as previously described (Saez-Orellana et al., 2018). Briefly, the cells were cultured in DMEM with 5% fetal bovine serum, 100 U/ml penicillin, 100 μg/ml streptomycin, 2 mM L-glutamine, and incubated under standard conditions (37 °C, 5% CO_2) until 80% of confluence was achieved. The cells were plated at a concentration of 50,000 cells/well.

4.2. Aβ aggregation

Human $Aβ_{1–42}$ labeled with FAM (green fluorescence) at its N-terminus, and unlabeled peptides were purchased from AnaSpec (CA, USA), and Aβ was purchased from GenicBio (China). The preparation and storage were performed as previously reported by our laboratory (Peters et al., 2016). Briefly, $Aβ_{1–42}$ was dissolved in hexafluoroisopropanol (HFIP), aliquoted, evaporated at room temperature and stored at −20 °C. To prepare the Aβ oligomers (80 μM), ultrapure water was added to the aliquots, and after 10–20 min incubation at room temperature the samples were stirred at 500 rpm using a Teflon-coated micro-stir bar for 24–48 h at room temperature (~22 °C) to form Aβ oligomers which were used immediately. The presence of Aβ oligomers in the preparation was checked by a silver stain gel that showed abundant species between 17 and 50 kDa (data not shown). In addition, transmission electron microscopy showed smaller-structured oligomers and the absence of fibers which readily appeared after longer incubations at 37 °C (Peters et al., 2016).

4.3. Aβ aggregation assay

The Aβ oligomers (32 μM) were incubated with and without the molecule (160 μM) in a 96 well plate for 20 h at 37 °C. Measurements were obtained every 2 min in a Novostar multi-reader (Labtech) with an absorbance filter of 482 nm, and data were integrated and analyzed with the Novostar software.

4.3.1. Circular dichroism of Aβ

Spectra of Aβ samples aggregated alone and with M30 were obtained on a Jasco J-815 spectrophotometer (Jasco, Japan) with a 100 nm/min scan speed. The data were recorded over 250 to 190 nm wavelengths at room temperature with a 10 mm length quartz cell. Aβ42 (1 μM) was aggregated with 0, 5, and 10 μM M30 to maintain a 1:1 and 1:5 ratio, respectively. The resulting spectra were corrected by subtracting the solvent background. Processed data were smoothed for better presentation. We measured the protein content in the cuvette before and after adding M30 to be sure that Aβ had not precipitated in solution when adding M30 using the colorimetric Protein Assay Kit BCA (Pierce). No noticeable changes were detected between the Aβ sample with and without M30 at both tested concentrations (5 and 10 μM). Because both Aβ and M30 have a similar absorbance in solution, this result indicates that the peptide is present in the cuvette and the observed change in the circular dichroism is related to a change in the secondary structure of the peptide due to the action of M30.

4.4. M30 molecule preparation

The molecule 2-Octahydroisoquinolin-2(1H)-ylethanamine (Matrix Scientific, USA) was dissolved in dimethyl sulfoxide (DMSO) to a final concentration of 10 mM, and aliquots were stored at −20 °C until use. For lower stock concentration, M30 was dissolved in ultrapure water or saline.

4.5. Structure-based virtual screening

A set of approximately 13,200,000 molecules belonging to the "Clean drug-like" subgroup were obtained from the ZINC database (UCSF, USA) and prepared to generate their minimized energy conformations and protonated states corresponding to pH 7 ± 0.2. Prior to docking simulations, ADME properties for all molecules were calculated with QuikProp (Schrödinger, LLC, NY, 2016) and then filtered according to the following requirements: no transgressions in Lipinski's rule of five or in Jorgensen's rule of three (Jorgensen and Duffy, 2002; Lipinski et al., 2001), ability to cross the blood-brain barrier [PlogBB > − 1] (Kelder et al., 1999), potential activity in the central nervous system [CNS ≥0] (Ajay et al., 1999), and not extensively

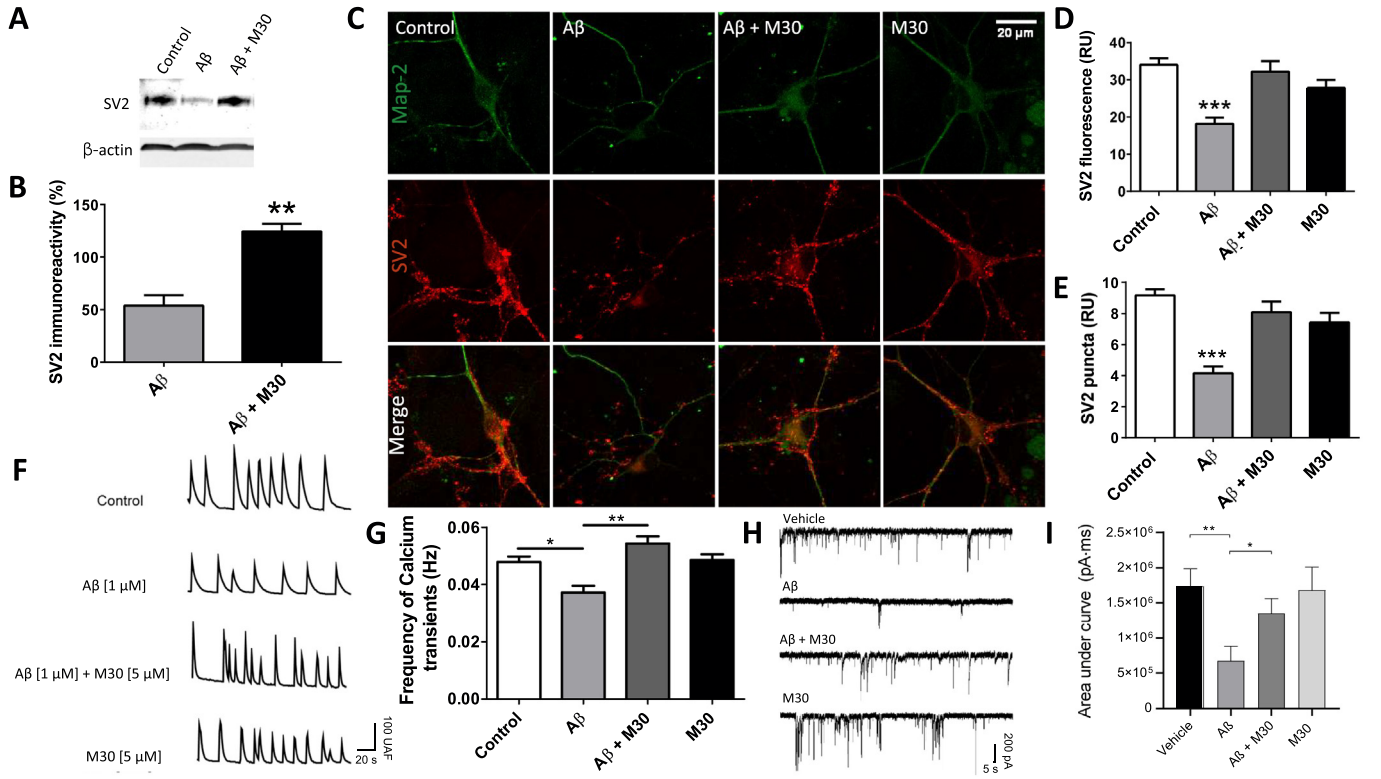

Fig. 7. M30 inhibited the synaptic toxicity induced by Aβ. (A) Western blots for SV2 after 24 h of incubation with Aβ (1 μM) and M30 (5 μM). The western blot for β-actin was used as a control for the amount of SV2 loaded. (B) SV2 normalized immunoreactivity from panel A taking the control value as 100%, $n = 4$. (C) Confocal microscopy shows SV2 (red) and MAP2 (green) after 24-h treatment with Aβ (1 μM) and M30 (5 μM). (D, E) SV2 fluorescence intensity and the number of punctas in primary processes per 20 μm from panel C. Number of primary processes quantified in Control (31 processes from/20 neurons), Aβ (24/14 neurons), Aβ + M30 (13/9 neurons), M30 (14/9 neurons). (F) M30 blocked the decrease in calcium transients induced by chronic application of Aβ (1 μM, 24 h) to hippocampal neurons. (G) Frequency of calcium transients from panel F. H) Representative traces of synaptic neurotransmission in hippocampal neurons after 48 h application of extracellular Aβ oligomers (1 μM), in the presence or absence of M30 (1 μM). I) Quantification of synaptic transmission from panel H, showing that the decrease in synaptic transmission induced by Aβ was blocked by M30. * $p < .05$, ** $p < .01$. *** $p < .001$. (For interpretation of the references to colour in this figure legend, the reader is referred to the web version of this article.)

metabolized in the body [#metab < 4]. Subsequently, we performed a massive docking protein-ligand with Glide using the selected molecules and the interaction grid created on the C-terminal (CT) of the Aβ monomer surface and centered on amino acids ^{32}I, ^{35}MV^{36}, ^{39}VVIA^{42} as centroid (Schrödinger, LLC, NY, 2016). Docking simulations, using 1IYT Aβ structure, were performed with the SP option of the Glide software that corresponds to the standard precision docking algorithm and in a second instance, they were refined using the XP algorithm which has a higher precision. Analysis of the Aβ/molecule interface by the same software including structural and energetic parameters generated a docking score used to rank all tested molecules. Additionally, an energy calculation was done using MM-GBSA for the best-ranked complexes with Prime software (Schrödinger, LLC, NY, 2016) to predict a theoretical ΔG_{bind}. Taken together, the docking score and ΔG_{bind} improved the description of the interaction between Aβ and the small molecules. Finally, selected molecules were evaluated in a second docking using a larger interaction grid including the central loop region (LP) to detect additional interaction sites on the surface of the Aβ monomer.

4.6. Molecular dynamics simulations

The M30 ligand was optimized at the Hatree-Fock/6-31G* level of theory using the Gaussian09 software. The generalized amber force field parameters of the ligand were obtained with the Antechamber program using partial charges from quantum chemical calculation based on the restrained electrostatic potential (RESP). Two poses of the M30 molecule obtained from the structure-based virtual screening procedure were used to generate two peptide systems: Aβ-M30(CT) and Aβ-M30(LP). The Aβ, Aβ-M30(CT), and Aβ-M30(LP) structures were solvated with approximately 13,600 TIP3P water in 500,070 Å^3 volume of the cubic box separately. Five independent molecular dynamic trajectories simulations were generated for each of the three peptide regions. The force field ff99SB-ILDN, which exhibits considerably better agreement with the NMR data, was used in our simulations [Lindorff-Larsen et al., 2010, https://doi.org/10.1002/prot.22711]. The energy of each system was initially minimized by using 500 steps of the steepest descent minimization method, subsequently followed by 500 steps of the conjugate gradient method with the peptide being constrained by using a 500 kcal/mol harmonic potential. The system was further minimized by using 1000 steps of the steepest descent followed by 1500 steps of the conjugate gradient minimization method without restraints. Once energy minimization was done, the system was equilibrated using two steps: first, an NVT (constant temperature) ensemble was employed for 20 ps, and the temperature was gradually increased from 0 to 300 K; second, NPT (constant pressure) ensemble was applied for 200 ps to reach the correct water density at 1 atm pressure. Each trajectory was a production run for 1000 ns using an NPT ensemble. Production data were collected every 20 ps. The length of all bonds was constrained by the SHAKE algorithm. The Particle Mesh Ewald (PME) method was used for the long-range electrostatic interactions, and a 10 Å cutoff range was used to calculate the electrostatic interactions. The Langevin thermostat was used to control the temperature. In overall, a total of 5000 ns (5 trajectories × 1000 ns) simulation of Aβ1–42, Aβ1–42-M30(CT) and Aβ1–42-M30(LP) were used. All of the analysis of the present work was carried out from 200 ns to 1000 ns. The secondary structure *per* residue of the peptide was calculated using the DSSP

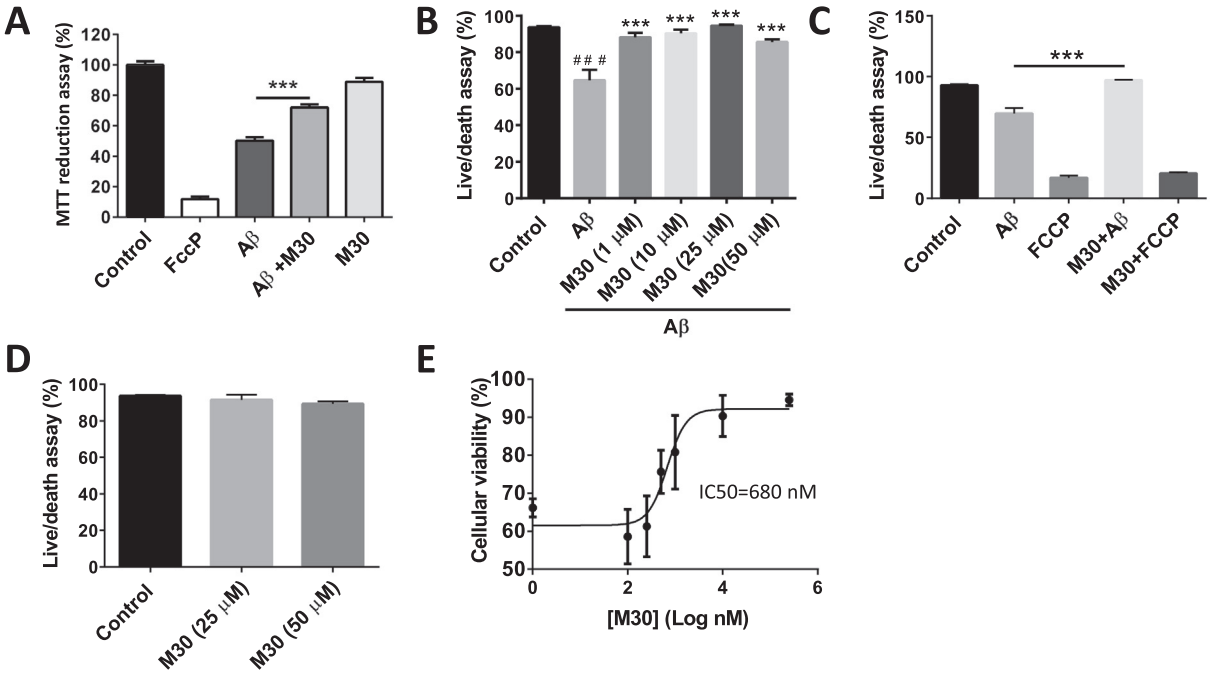

Fig. 8. M30 decreased Aβ-induced mitochondrial dysfunction and cytotoxicity. (A) The data shows MTT reduction assays obtained in PC12 cells treated with Aβ (1 μM) alone, FCCP (10 μM, positive control) and M30 (5 μM) with and without Aβ for 24 h. (B) Live/dead assay shows the effect in hippocampal neurons of Aβ (1 μM, 96 h) and Aβ plus different concentrations of M30 (1, 10, 25 and 50 μM). (C) Live/dead assay shows that in hippocampal neurons, M30 (5 μM) only blocked the toxicity induced by Aβ, but not FCCP. (D) M30 does not have intrinsic toxicity at 25 and 50 μM after 96 h treatment in hippocampal neurons. (E) Concentration curve of M30 to achieve the reduction in Aβ toxicity after 96 h treatment. The results are from at least 4 independent measurements, *** $p < .001$.

program. The root-mean-square deviation (RMSD) of the Cα atoms as a function of time is shown in Fig. S1 (Fig. S1). The RMSD values were stable for all peptides after 200 ns of simulation. After this time, the RMSD of all the systems fluctuated around its equilibrium value. We calculated the distance between the center of mass of M30 and different regions of the peptides using the 'distance' program in Amber. Salt-bridges were identified between positively charged amino acids Arg5, Lys16, and Lys28, and negatively charged amino acids Asp1, Glu3, Asp7, Glu11, Glu22, and Asp23. We considered a salt bridge between two charged residues when the distance between two specific atoms was below 4.5 Å. The salt bridges between positively and negatively charged residues were determined by the following equation.

$$SB = \sum_{i,j} S_{i,j}$$

$$S_{i,j} = 1 \; if \; r_{i,j} \leq 0$$

$$S_{i,j} = 0 \; if \; r_{i,j} > 0$$

$$r_{i,j} = |r_i - r_j| - d_0$$

where i and j relate to Nζ (Lys), Nη (Arg), Cγ (Asp), and Cδ (Glu). d_0 is the distance between atoms i and j. The value of d_0 was 4.5 Å. Molecular dynamics simulations were performed using the Amber16 package.

4.7. Calcium imaging

Hippocampal neurons were loaded with Fluo-8 AM (1 μM in pluronic acid/DMSO, Abcam, USA) for 30 min at 37 °C and then washed twice with external solution (in mM: 150 NaCl, 5.4 KCl, 2.0 $CaCl_2$, 1.0 $MgCl_2$, 10 glucose, and 10 HEPES (pH 7.4)). Cells were mounted in a perfusion chamber that was placed on the stage of an inverted fluorescent microscope (Eclipse TE, Nikon) equipped with a xenon lamp and a 40× objective (22–24 °C) and subsequently illuminated for 200 ms using a computer-controlled Lambda 10–2 filter wheel (Sutter Instruments) and regions of interest were simultaneously selected on neuronal somata containing Fluo-8 fluorescence (absorption 490 nm and emission 514 nm) in a field having usually more than 10 cells. For transient recordings, images were collected at 1 s intervals during a continuous 200-s period of recording with a 12-bit cooled SensiCam camera (PCO, Germany). Finally, calcium transients were acquired and analyzed offline with Axon Instruments Workbench 2.2 software.

For long-term recordings in PC12 cells, a multi-reader plate (Novostar, Labtech) in fluorescence mode was used, measuring the total fluorescence of each well every 2 min for 10 min at 37 °C and after that, Aβ oligomers (1 μM) with or without M30 (5 μM) were injected and data was recorded for 40 min.

4.8. MTT reduction assay

PC12 cells were incubated with MTT solution (0.5 mg/ml) for 3 h, and the precipitate of the reduced MTT was dissolved using DMSO for 5 min. Absorbance was measured in a multiplate reader (NovoStar, LabTech) at wavelengths of 560 nm and 620 nm, and was quantified using NovoStar Software for the different experimental conditions.

4.9. Live/dead assay

The protocol was followed as previously described (Araya et al., 2014). Hippocampal neurons were incubated for 96 h with Aβ (1 μM), vehicle control, M30, or a potent mitochondrial oxidative phosphorylation uncoupler FCCP as a positive control for death. After the treatment, neurons were washed with PBS (Gibco, USA) and then treated with Calcein-AM and Ethidium homodimer-1 (EthD-1) for 30 min at 37 °C, as described by the manufacturer (Invitrogen, Carlsbad, CA, USA). After a final wash with PBS, the EthD-1 emission was detected at 635 nm and calcein at 515 nm in a multiplate reader (Novostar). An increase in red fluorescence reflected an increase in neuronal death, while an increment in the green signal indicated more viable neurons.

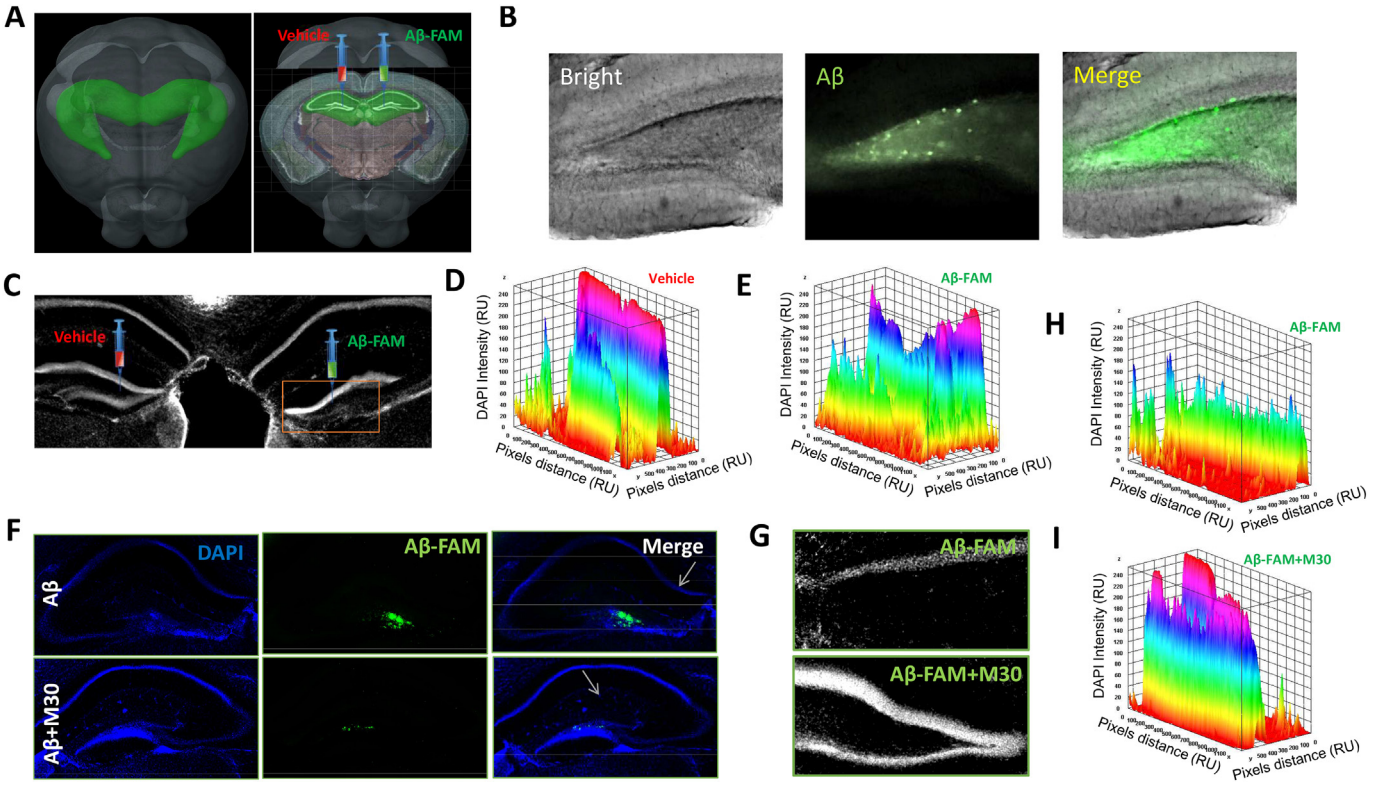

Fig. 9. Neuroprotective effects of M30 following injection of Aβ in the dentate gyrus. (A) Shows a mouse brain from the Allen Brain Institute showing the hippocampus in green. The image on the right shows the stereotaxic procedure, injecting the dentate gyrus (DG) of the left hemisphere with the vehicle, and the right DG with Aβ-FAM (4 μl of Aβ 80 μM). (B) Coronal section of the injected DG showing Aβ-FAM after 1 day. (C) Coronal image showing DAPI staining after 2 weeks of Aβ-FAM injection into the DG. (D, E) Quantification of Aβ-FAM from data in C for DAPI positive cells in the DG injected with the vehicle and Aβ-FAM respectively. (F) The top images show Aβ-FAM (green) in the DG at 2 weeks post injection, while the bottom panel of images are of Aβ-FAM plus M30 (4 μl, 80 μM). (G) M30 protected the DG from Aβ-FAM induced toxicity, shown by the increased presence of DAPI positive cells. (H, I) panel H is the quantification from data in G for DAPI positive neurons in panel G. (For interpretation of the references to colour in this figure legend, the reader is referred to the web version of this article.)

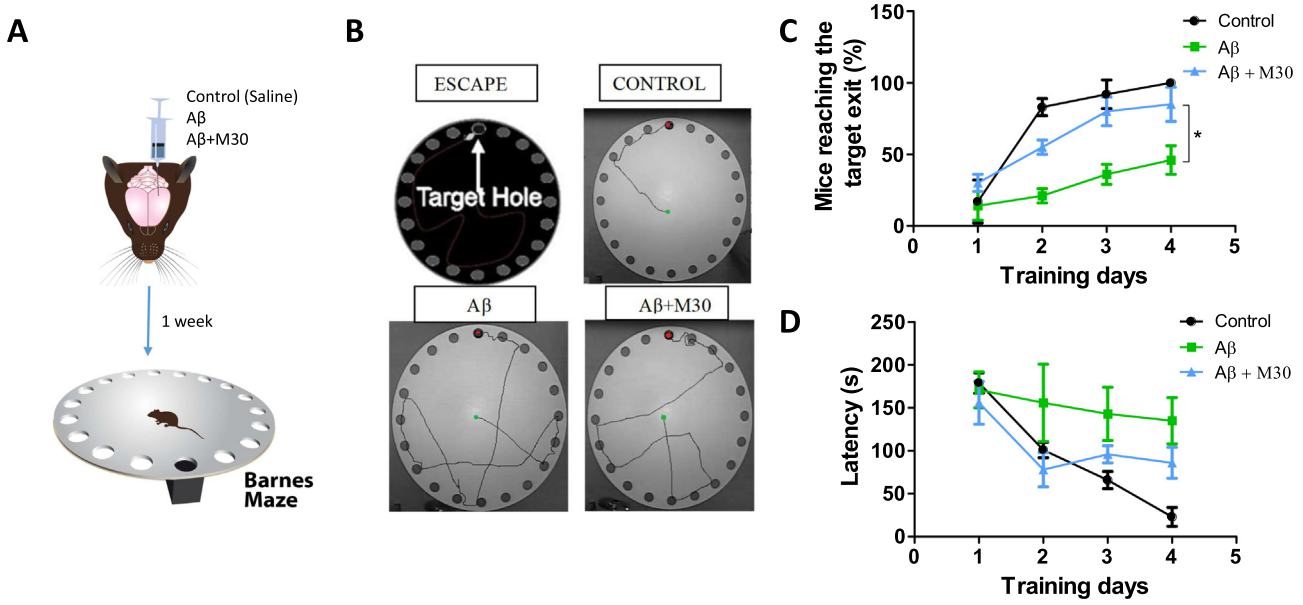

Fig. 10. M30 improves spatial learning and memory disruption by Aβ. (A) Scheme of the protocol for spatial learning and memory test. Saline, Aβ or Aβ + M30 were injected bilaterally (see methods) into the DG and the Barnes Maze protocol was performed following 1 week. (B) Representative tracking of the animals around the maze. (C, D) Plots showing the percentage of mice reaching the exit (before 3 min) and latency during the training days. Control ($n = 6$), Aβ ($n = 7$) and Aβ + M30 ($n = 5$). * denotes $p < .05$.

4.10. Immunofluorescence

Hippocampal neurons plated in 35 mm dishes were washed in phosphate-buffered saline (PBS; pH 7.4) and fixed with 4% paraformaldehyde for 15 min. Then, the neurons were washed again in PBS, and the cells were permeabilized and blocked for 30 min with PBST (triton X-100 0.1% in PBS) plus 10% bovine serum albumin. Subsequently, cells were incubated with the following primary antibodies between 16 and 24 h: anti-MAP2, 1:400 (Santa Cruz Biotechnology), and anti-SV2 1:200 (Santa Cruz Biotechnology). Secondary antibodies conjugated with FITC, Cy3, and/or Cy5 at a dilution of 1:200 for 2 h were used for fluorescent staining (Jackson ImmunoResearch Laboratories, PA). Finally, samples were mounted in fluorescent mounting medium (DAKO, CA, USA) and images were obtained using a Nikon Eclipse confocal microscope (Nikon, Japan). The immunoreactivity of the proteins was quantified at primary processes with ImageJ software (NIH).

4.11. Dot blots and Western assays

For dot blots, the cells were lysed after treatment with a buffer containing 0.5 mM EDTA, 140 mM NaCl, 0.5%Triton X-100, and 100 mM DTT. Equal amounts of proteins were added to a nitrocellulose membrane and dried. Unspecific sites were blocked with 5% milk and incubated with the primary anti-Aβ antibody (1:1000; Santa Cruz Biotechnology). Then, secondary antibodies conjugated with horseradish peroxidase (1:5000 dilution; Santa Cruz Biotechnology) were added and visualized with an ECL Plus Western Blotting Detection System (PerkinElmer, MA, USA).

For western blots, equal amounts of proteins were separated using 10% sodium dodecyl sulfate-polyacrylamide gel electrophoresis as previously described (Peters et al., 2011). Protein bands were transferred onto nitrocellulose membranes, blocked with 5% milk, and incubated with the primary anti-SV2 antibody (1:200; Developmental Studies Hybridoma Bank, Iowa City, IA) for 24 h at 4 °C. A secondary antibody conjugated with horseradish peroxidase (1:5000; Santa Cruz Biotechnology) was incubated for 2 h and visualized with an ECL Plus Western Blotting Detection System (PerkinElmer). The western blot for β-actin, a house keeping marker, was used as a control for the amount of SV2 loaded. This is particularly important to normalize signal variations like in Fig. 7A.

4.12. Electrophysiology

Electrophysiological recordings were carried out using the patch-clamp technique as previously described (Peters et al., 2015). Briefly, after neuronal treatment for 48 h with Aβ (1 μM) or Aβ + M30 (1 μM), the culture media was changed for an external solution containing (in mM): 150 NaCl, 5.4 KCl, 2.0 $CaCl_2$, 1.0 $MgCl_2$, 10 glucose, and 10 HEPES (pH 7.4). The internal solution consisted of (in mM): 120 KCl, 2.0 $MgCl_2$, 2 ATP−Na_2, 10 BAPTA, 0.5 GTP, 10 HEPES (pH 7.4). The holding potential was fixed at −60 mV, and postsynaptic currents were acquired at 50 ms intervals using a Digidata 1200 board and the pClamp10 software (Axon Instruments, Inc). Recording pipettes were pulled from borosilicate glass (WPI, Sarasota, FL) on a horizontal puller (Sutter Instruments, Novato, CA) having a resistance between 5 and 7 MΩ.

4.13. Stereotaxic injections

Stereotaxic injections were followed as previously described (Jean, 2015). Briefly, vehicle, Aβ-FAM (4 μl, 80 μM), or Aβ + M30 (4 μl, 80 μM) was injected into the DG of the hippocampus according to the brain coordinates obtained from "The mouse brain in stereotaxic coordinates": AP -2.00 mm, ML ± 1.3 mm, DV -2.2 mm (Paxinos and Franklin, 2001). For the cellular staining, injections of Aβ were made in one hemisphere, while the other hemisphere was injected with Aβ + M30 in order to reduce the dispersion between control and treatment. After 2 weeks post-surgery, the mouse was anesthetized with isoflurane and decapitated, and the brain removed and sliced with a vibratome (Leica, Germany). Once the hippocampal slices were obtained and fixed with 4% paraformaldehyde, the nucleus of the cells was stained with DAPI and visualized with confocal microscopy. The number or density of DAPI positive cells was analyzed and neuronal death was reflected by a decrease in the number of DAPI positive cells (Jean, 2015).

4.14. Memory and learning test

For memory and learning studies, male and female C57BL/J6 mice (20–30 g; 6 to 12 months) were used in the Barnes Maze assay. Basically, the study consists of a circular platform with a maximum of 20 holes around its circumference, in which visual cues, such as shapes or patterns of colour, are placed around the table in plain sight of the animal. Beneath one of the holes, there is an "escape box" to which the mouse can access through the corresponding hole on the top of the table. The model is based on the aversion of rodents to open spaces which causes the mouse to take refuge in the escape box. A rodent after 4 or 5 trials will go directly to the escape hole without trying to escape through the wrong holes. However, an impaired mouse will take much longer to "learn" the location of the escape hole. To induce escape behavior, we used a bright light that is aversive to rodents and increases their motivation to go into a safe place. The escape box was maintained at a fixed location for the duration of the training, which involved multiple daily trials spread over several days.

4.15. Data analyses

The values are expressed as mean ± standard error mean (± SEM). The nonlinear analysis was performed using Prism (GraphPad Software, Inc). Statistical differences were determined using Student's *t*-test, and data with more than two groups or factors were analyzed by one-way ANOVA test followed by a Bonferroni *post hoc* test. Values for $*p < .05$, $**p < .01$ and $***p < .001$ were considered statistically significant. All the experiments were performed at least in triplicate.

Acknowledgments

We thank Lauren Aguayo for revising the manuscript and for technical assistance. We also thank Ixia Cid for technical support, Cecilia Gonzalez for graphic design and Centro de Microscopía Avanzada del BíoBío (PIA ECM12) for microscopy imaging support. This work was supported by FONDECYT 1140473, 1180752 (LGA) and CONICYT-FONDEQUIP-EQM160063 (WG).

Appendix A. Supplementary data

Supplementary data to this article can be found online at https://doi.org/10.1016/j.nbd.2020.104938.

References

Ajay, et al., 1999. Designing libraries with CNS activity. J. Med. Chem. 42, 4942–4951.
Aguayo, L.G., Pancetti, F.C., 1994. Ethanol modulation of the gamma-aminobutyric acidA- and glycine-activated cl- current in cultured mouse neurons. J. Pharmacol. Exp. Ther. 270, 61–69.
Araya, J.A., et al., 2014. Modulation of neuronal nicotinic receptor by quinolizidine alkaloids causes neuroprotection on a cellular Alzheimer model. J. Alzheimers Dis. 42, 143–155.
Autiero, I., et al., 2013. In silico investigation and targeting of amyloid beta oligomers of different size. Mol. BioSyst. 9, 2118–2124.
Baleriola, J., et al., 2014. Axonally synthesized ATF4 transmits a neurodegenerative signal across brain regions. Cell. 158, 1159–1172.

Banting, F.G., et al., 1922. Pancreatic extracts in the treatment of diabetes mellitus. Can. Med. Assoc. J. 12, 141–146.
Bitan, G., et al., 2003. Elucidation of primary structure elements controlling early amyloid beta-protein oligomerization. J. Biol. Chem. 278, 34882–34889.
Carreiras, M.C., et al., 2013. The multifactorial nature of Alzheimer's disease for developing potential therapeutics. Curr. Top. Med. Chem. 13, 1745–1770.
Colvin, M.T., et al., 2016. Atomic resolution structure of monomorphic Abeta42 amyloid fibrils. J. Am. Chem. Soc. 138, 9663–9674.
De Strooper, B., Chavez Gutierrez, L., 2015. Learning by failing: ideas and concepts to tackle gamma-secretases in Alzheimer's disease and beyond. Annu. Rev. Pharmacol. Toxicol. 55, 419–437.
Grover, S., et al., 2014. Computational identification of novel natural inhibitors of glucagon receptor for checking type II diabetes mellitus. BMC Bioinformatics 15 (Suppl. 16), S13.
Guivernau, B., et al., 2016. Amyloid-beta peptide Nitrotyrosination stabilizes oligomers and enhances NMDAR-mediated toxicity. J. Neurosci. 36, 11693–11703.
Huang, T.H., et al., 2000. Structural studies of soluble oligomers of the Alzheimer beta-amyloid peptide. J. Mol. Biol. 297, 73–87.
Jean, Y.Y., et al., 2015. Stereotaxic infusion of oligomeric amyloid-beta into the mouse hippocampus. J Vis Exp. 100, e52805.
Jin, M., et al., 2011. Soluble amyloid beta-protein dimers isolated from Alzheimer cortex directly induce tau hyperphosphorylation and neuritic degeneration. Proc. Natl. Acad. Sci. U. S. A. 108, 5819–5824.
Jorgensen, W.L., Duffy, E.M., 2002. Prediction of drug solubility from structure. Adv. Drug Deliv. Rev. 54, 355–366.
Kelder, J., et al., 1999. Polar molecular surface as a dominating determinant for oral absorption and brain penetration of drugs. Pharm. Res. 16, 1514–1519.
Lau, J.L., Dunn, M.K., 2018. Therapeutic peptides: historical perspectives, current development trends, and future directions. Bioorg. Med. Chem. 26, 2700–2707.
Lindorff-Larsen, K., Piana, S., Palmo, K., Maragakis, P., Klepeis, J.L., Dror, R.O., Shaw, D.E., 2010. Improved side-chain torsion potentials for the Amber ff99SB protein force field. Proteins 78 (8), 1950–1958.
Lipinski, C.A., et al., 2001. Experimental and computational approaches to estimate solubility and permeability in drug discovery and development settings. Adv. Drug Deliv. Rev. 46, 3–26.
Ono, K., et al., 2009. Structure-neurotoxicity relationships of amyloid beta-protein oligomers. Proc. Natl. Acad. Sci. U. S. A. 106, 14745–14750.
O'Nuallain, B., et al., 2010. Amyloid beta-protein dimers rapidly form stable synaptotoxic protofibrils. J. Neurosci. 30, 14411–14419.
Parodi, J., et al., 2010. Beta-amyloid causes depletion of synaptic vesicles leading to neurotransmission failure. J. Biol. Chem. 285, 2506–2514.
Paxinos, G., Franklin, K.B.J., 2001. The Mouse Brain in Stereotaxic Coordinates, 2nd Edition. Academic Press, San Diego.
Peters, C., et al., 2011. Biphasic effects of copper on neurotransmission in rat hippocampal neurons. J. Neurochem. 119, 78–88.
Peters, C., et al., 2013. Inhibition of amyloid beta-induced synaptotoxicity by a pentapeptide derived from the glycine zipper region of the neurotoxic peptide. Neurobiol. Aging 34, 2805–2814.
Peters, C., et al., 2015. Alzheimer's Abeta interacts with cellular prion protein inducing neuronal membrane damage and synaptotoxicity. Neurobiol. Aging 36, 1369–1377.
Peters, C., et al., 2016. Differential membrane toxicity of amyloid-beta fragments by pore forming mechanisms. J. Alzheimers Dis. 51, 689–699.
Riek, R., Eisenberg, D.S., 2016. The activities of amyloids from a structural perspective. Nature. 539, 227–235.
Saez-Orellana, F., et al., 2018. P2X receptor overexpression induced by soluble oligomers of amyloid beta peptide potentiates synaptic failure and neuronal dyshomeostasis in cellular models of Alzheimer's disease. Neuropharmacology. 128, 366–378.
Sakono, M., Zako, T., 2010. Amyloid oligomers: formation and toxicity of Abeta oligomers. FEBS J. 277, 1348–1358.
Salomone, S., et al., 2012. New pharmacological strategies for treatment of Alzheimer's disease: focus on disease modifying drugs. Br. J. Clin. Pharmacol. 73, 504–517.
Sandberg, A., et al., 2010. Stabilization of neurotoxic Alzheimer amyloid-beta oligomers by protein engineering. Proc. Natl. Acad. Sci. U. S. A. 107, 15595–15600.
Sepulveda, F.J., et al., 2010. Synaptotoxicity of Alzheimer beta amyloid can be explained by its membrane perforating property. PLoS One 5, e11820.
Shankar, G.M., et al., 2007. Natural oligomers of the Alzheimer amyloid-beta protein induce reversible synapse loss by modulating an NMDA-type glutamate receptor-dependent signaling pathway. J. Neurosci. 27, 2866–2875.
Trippier, P.C., et al., 2013. Target- and mechanism-based therapeutics for neurodegenerative diseases: strength in numbers. J. Med. Chem. 56, 3121–3147.
Tycko, R., 2011. Solid-state NMR studies of amyloid fibril structure. Annu. Rev. Phys. Chem. 62, 279–299.
Veeramachaneni, G.K., et al., 2015. High-throughput virtual screening with e-pharmacophore and molecular simulations study in the designing of pancreatic lipase inhibitors. Drug Des Devel Ther. 9, 4397–4412.
Webster, S.J., et al., 2014. Using mice to model Alzheimer's dementia: an overview of the clinical disease and the preclinical behavioral changes in 10 mouse models. Front. Genet. 5, 88.